Finite Volume Implementation of Non-Dispersive, Non-Hydrostatic Shallow Water Equations

Vincent Guinot, Didier Clamond, Denys Dutykh

Finite Volume Implementation of Non-Dispersive, Non-Hydrostatic Shallow Water Equations

Vincent Guinot, Didier Clamond and Denys Dutykh

Abstract A shock-capturing, finite volume implementation of recently proposed non-hydrostatic two-dimensional shallow water equations, is proposed. The discretization of the equations in conservation form implies the modification of the time derivative of the conserved variable, in the form of a mass/inertia matrix, and extra terms in the flux functions. The effect of this matrix is to slow down wave propagation in the presence of significant bottom slopes. The proposed model is first derived in conservation form using mass and momentum balance principles. Its finite volume implementation is then presented. The additional terms to the shallow water equations can be discretized very easily via a simple time-stepping procedure. Two application examples are presented. These examples seem to indicate that the proposed model does not exhibit strong differences with the classical hydrostatic shallow water model under steady-state conditions, but that its behavior is significantly different when transients are involved.

Keywords Shallow water model · Non-hydrostatic pressure distribution · Bottom acceleration

V. Guinot (✉)
Université Montpellier—HSM UMR 5569, Place Eugène Bataillon, CC 057, Montpellier Cedex 5, 34095, Montpellier, France
e-mail: guinot@msem.univ-montp2.fr

D. Clamond
Université de Nice-Sophial Antipolis—Laboratoire J. A, Dieudonné UMR 7351, Parc Valrose, Nice Cedex 02, 06108, Nice Cedex, France
e-mail: didierc@unice.fr

D. Dutykh
LAMA UMR 5127, Campus Scientifique, Le-Bourget-du-Lac Cedex 73376 Marseilles Cedex, France
e-mail: Denys.Dutykh@univ-savoie.fr

P. Gourbesville et al. (eds.), *Advances in Hydroinformatics*,
Springer Hydrogeology, DOI: 10.1007/978-981-4451-42-0_17,

1 Introduction

Among the many available tools for water wave model formulation (see [1] for an overview), the variational formulation has proved a powerful one [2, 3]. Recently, the Lagrangian variational approach has been used to derive a family of free surface flow models [1, 4]. This approach allows the classical shallow water equations, the Serre equations, the Boussinesq equations, and many others, to be derived as particular cases [1].

The purpose of this communication is to show how a non-hydrostatic shallow water model, presented in [4] under the assumption of non-negligible flow vertical acceleration, can be implemented in a simple way within a classical, Godunov-type algorithm. This model has the interesting property that the system of governing equations remains hyperbolic, thus making standard numerical techniques easily applicable.

In Sect. 2, the governing equations are derived in conservation form, not using the variational approach, but using the more classical integral form for mass and momentum balances that are more widely accepted by the hydraulic community. In Sect. 3, an overview of the numerical implementation is given. Section 4 is devoted to computational examples and Sect. 5 to the conclusions.

2 Assumptions and Governing Equations

2.1 Notation—Assumptions

The following notation is used (Fig. 1). The water depth is denoted by h, and the vertical averages of the x- and y-components of the flow velocity are denoted, respectively, by u and v. The bottom and free surface elevations are denoted, respectively, by z_b and z_s, and $z_s = z_b + h$. The unit discharge in the x- and y-directions is denoted, respectively, by $q = hu$ and $r = hv$. The bottom slopes in the x- and y- directions are denoted, respectively, by $S_{0,x}$ and $S_{0,y}$. $\mathbf{u} = [u, v, w]^T$ is the flow velocity vector. The restriction of the velocity vector to the horizontal plane is defined as $\mathbf{u}_h = [u, v]^T$.

The classical shallow water equations are based on the following assumptions:

(A1) the water in incompressible,

(A2) the flow velocity is uniform over the depth,

(A3) the pressure distribution is hydrostatic over the vertical,

(A4) the bottom slope is negligible.

In the modified shallow water equations, assumptions (A1–3) are retained, but assumption (A4) is replaced with the following one:

(A5) the bottom slope may not be negligible, and the flow velocity vector is collinear to the bottom tangent vector.

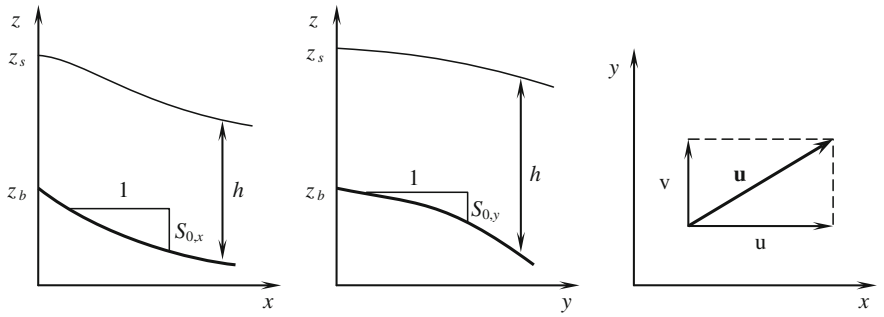

Fig. 1 Notation vertical cross-section in the (x, z) plane (*left*), in the (y, z) plane (*middle*), and in the (x, y) plane (*right*)

Assumption (A4) may be translated mathematically as follows:

$$\tilde{w}(x,y,z,t) = w(x,y,t) = \mathbf{u}_h(x,y,t).\nabla z_b = -u(x,y,t)S_{0,x} - v(x,y,t)S_{0,y} \ \forall z \in [z_b; z_s] \tag{1}$$

where $\tilde{w}(x,y,z,t)$ is the vertical component of the flow velocity vector. Equation (1) has important consequences on the momentum source term in the conservation form of the equations.

2.2 Conservation Form

In [1, 4], the governing equations are derived using variational principles. Owing to the non-uniqueness of weak solutions (see [5] for the example of the shallow water equations), it is not clear whether the conservation form established in [1, 4] using variational principles remains valid in the presence of flow discontinuities. For this reason, the governing equations are derived using the integral form of mass and momentum balances over a control volume hereafter.

The continuity equation is derived by carrying out a mass balance over a cylindrical control volume Ω, extending from the bottom to the free surface (Fig. 2).

The boundary Γ of the control volume being vertical, its normal unit vector $\mathbf{n}$ (oriented outwards) lies in the (x, y) plane. Mass conservation with assumption (A1) gives, after simplification by the (constant) water density,

$$\partial_t \int_{\Omega} \mathrm{d}\Omega + \int_{\Gamma} \mathbf{u}.\mathbf{n}\, d\Gamma = 0 \tag{2}$$

Since the boundary is vertical, $\mathrm{d}\Gamma = h\,\mathrm{d}s$, where s is the curvilinear coordinate along the boundary, and $\mathrm{d}\Omega = h\,\mathrm{d}A$, where $\mathrm{d}A$ is the infinitesimal area in plan view. Introducing these definitions into (2) yields

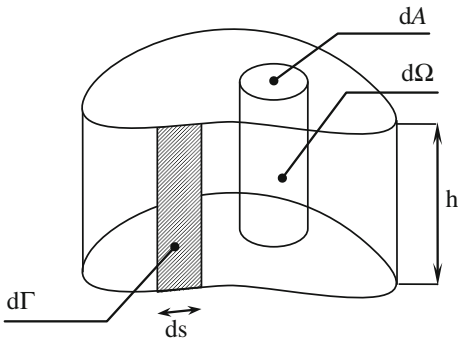

Fig. 2 Definition sketch for the integration control volume

$$\partial_t \int_\Omega h \, \mathrm{d}A + \int_\Gamma h\mathbf{u}.\mathbf{n} \, \mathrm{d}s = 0 \tag{3}$$

which yields the well-known differential form

$$\partial_t h + \nabla.(h\mathbf{u}_h) = 0 \tag{4}$$

where $\mathbf{u}_h$ is the restriction of $\mathbf{u}$ to the horizontal plane.

The momentum equation is obtained from Euler's theorem:

$$\partial_t \int_\Omega h\mathbf{u}\mathrm{d}A + \int_\Gamma (\mathbf{u}.\mathbf{n})h\mathbf{u} \, \mathrm{d}s = \int_\Omega \mathbf{g}h\mathrm{d}A - \int_\Gamma \frac{g}{2}h^2\mathbf{n} \, \mathrm{d}s + \mathbf{R} \tag{5}$$

where $\mathbf{g} = [0, 0, -g]^T$ is the gravitational acceleration and $\mathbf{R} = [R_x, R_y, R_z]^T$ is the reaction of the bottom. A major difference with the classical shallow water equations is that owing to assumption (A5), the terms R_x and R_y in Eq. (5) are modified. Projecting (5) onto the three axes, using the fact that $\mathbf{R}$ is collinear to the normal unit vector to the bottom yields:

$$\partial_t \int_\Omega hu\mathrm{d}A + \int_\Gamma q_n u \, \mathrm{d}s = -\int_\Gamma \frac{g}{2}h^2 n_x \, \mathrm{d}s + R_z S_{0,x} \tag{6}$$

$$\partial_t \int_\Omega hv\mathrm{d}A + \int_\Gamma q_n v \, \mathrm{d}s = -\int_\Gamma \frac{g}{2}h^2 n_y \, \mathrm{d}s + R_z S_{0,y} \tag{7}$$

$$\partial_t \int_\Omega hw\mathrm{d}A + \int_\Gamma q_n(\mathbf{u}_h.\nabla z_b) \, \mathrm{d}s = \int_\Omega -gh \, \mathrm{d}A + R_z \tag{8}$$

where q_n is the normal unit discharge to the boundary. Equations (1) and (8) lead to the following expression for R_z:

$$R_z = \int_\Omega \left(\partial_t(hw) + gh\right) \mathrm{d}A + \int_\Gamma q_n(\mathbf{u}_h.\nabla z_b)\ \mathrm{d}s$$
$$= \int_\Omega \left(gh + \partial_t(h\mathbf{u}_h).\nabla z_b\right) \mathrm{d}A + \int_\Gamma q_n(\mathbf{u}_h.\nabla z_b)\ \mathrm{d}s \tag{9}$$

It is easy to see from Eq. (9) that the assumption of a non-negligible bottom slope introduces an additional vertical acceleration, thus yielding a modification in the apparent gravitational acceleration. Substituting Eq. (9) into (6–7) leads to

$$\partial_t \int_\Omega h\left(u + \mathbf{u}_h.\nabla z_b S_{0,x}\right) \mathrm{d}A + \int_\Gamma \left(u + \mathbf{u}_h.\nabla z_b S_{0,x}\right) q_n\ \mathrm{d}s$$
$$= -\int_\Gamma \frac{g}{2} h^2 n_x\ \mathrm{d}s + \int_\Omega ghS_{0,x}\mathrm{d}A \tag{10}$$

$$\partial_t \int_\Omega h\left(v + u + \mathbf{u}_h.\nabla z_b S_{0,y}\right)\mathrm{d}A + \int_\Gamma \left(v + \mathbf{u}_h.\nabla z_b S_{0,y}\right) q_n\ \mathrm{d}s$$
$$= -\int_\Gamma \frac{g}{2} h^2 n_y\ \mathrm{d}s \int_\Omega ghS_{0,y}\mathrm{d}A \tag{11}$$

thus yielding the following system in differential conservation form:

$$\partial_t \mathbf{M}\mathbf{U} + \partial_x \mathbf{F}_x + \partial_y \mathbf{F}_y = \mathbf{S} \tag{12}$$

$$\mathbf{U} \equiv \begin{bmatrix} h \\ q \\ r \end{bmatrix}, \mathbf{F}_x \equiv \begin{bmatrix} q \\ q^2/h + gh^2/2 + \left(\mathbf{u}_h.\nabla z_b S_{0,x}\right)q \\ qr/h + \left(\mathbf{u}_h.\nabla z_b S_{0,x}\right)r \end{bmatrix}, \mathbf{F}_y \equiv \begin{bmatrix} r \\ qr/h + \left(\mathbf{u}_h.\nabla z_b S_{0,y}\right)q \\ r^2/h + gh^2/2 + \left(\mathbf{u}_h.\nabla z_b S_{0,y}\right)r \end{bmatrix},$$
$$\mathbf{S} \equiv \begin{bmatrix} 0 \\ ghS_{0,x} \\ ghS_{0,y} \end{bmatrix}, \mathbf{M} \equiv \begin{bmatrix} 1 & 0 & 0 \\ 0 & 1 + S_{0,x}^2 & S_{0,x}S_{0,y} \\ 0 & S_{0,x}S_{0,y} & 1 + S_{0,y}^2 \end{bmatrix} \tag{13}$$

The appearance of the mass (or inertia) matrix $\mathbf{M}$ and two additional flux terms is worth noting. It is responsible for the modification in the wave propagation speeds as identified in [1, 4].

3 Shock-Capturing Finite Volume Discretization

The governing equations in conservation form (12–13) were implemented into a shock-capturing, finite volume-based computational code for shallow water simulations, the SW2D platform. This platform may be used to solve the shallow water equations with single porosity [6, 7] and multiple porosity [8], as well as the

two-dimensional shallow water sensitivity equations [9]. The Godunov-based solution techniques implemented in this implementation use MUSCL-based reconstructions [10] over unstructured grids. For the sake of computational rapidity, the eigenvector-based reconstruction [11] is used. It allows second-order time integration within a single timestep. The fluxes are computed using a modified HLLC [12] solver [7].

In a first step, the classical shallow water equations are solved:

$$\partial_t \mathbf{U} + \partial_x \mathbf{F}_x^{\mathrm{SW}} + \partial_y \mathbf{F}_y^{\mathrm{SW}} = \mathbf{S} \tag{14}$$

where $\mathbf{F}_x^{\mathrm{SW}} = [q, q^2/h + gh^2/2, qr/h]^T$ and $\mathbf{F}_y^{\mathrm{SW}} \equiv [r, qr/h, r^2/h + gh^2/2]^T$ are the classical shallow water fluxes. The discretization technique is a standard one and will not be described here for the sake of conciseness (see e.g., [13] for an overview).

In a second step, the additional terms in the fluxes are accounted for

$$\partial_t \mathbf{U} + \partial_x \mathbf{F}_x^{\mathrm{NH}} + \partial_y \mathbf{F}_y^{\mathrm{NH}} = 0 \tag{15}$$

where $\mathbf{F}_x^{\mathrm{NH}} = \left[0, \mathbf{u}_h.\nabla z_b S_{0,x} q, \mathbf{u}_h.\nabla z_b S_{0,x} r\right]^T$ and $\mathbf{F}_y^{\mathrm{NH}} = \left[0, \mathbf{u}_h.\nabla z_b S_{0,y} q, \mathbf{u}_h.\nabla z_b S_{0,y} r\right]^T$ are the additional fluxes arising from the non-hydrostatic assumption. Since these fluxes account for advection of the scalar quantity $\mathbf{u}_h.\nabla z_b$, a simple upwind flux formula is used, with the mass flux computed in step 1 using the modified Riemann solver.

In a third step, the influence of the inertia matrix is incorporated. This is done as follows: denoted by $\mathbf{U}_i^n$ the average cell value of $\mathbf{U}$ over the cell i at the time level n. Solving Eqs. (14–15) over the timestep Δt yields a provisional solution $\mathbf{U}_i^{n+1,(1)}$ at the time level n. The final solution $\mathbf{U}_i^{n+1}$ at the end of the timestep (thus, at time level $n + 1$) is given by

$$\mathbf{U}_i^{n+1} \approx \mathbf{U}_i^n + \Delta t\, \partial_t \mathbf{U} \approx \mathbf{U}_i^n + M^{-1}\left(\mathbf{U}_i^{n+1,(1)} - \mathbf{U}_i^n\right) \tag{16}$$

4 Application Examples

4.1 Steady-State Simulation

A steady-state experiment was carried out using the experimental facilities at the SupAgro'Montpellier engineering school. A Venturi flume with variable bottom was placed in a channel, and a constant discharge was prescribed upstream (Fig. 3).

The Venturi flume was operated under undrowned conditions, so that the flow velocity (hence the accelerations) be maximum. A constant discharge $Q = 40$ L s^{-1} was prescribed, and the free surface elevation was measured every

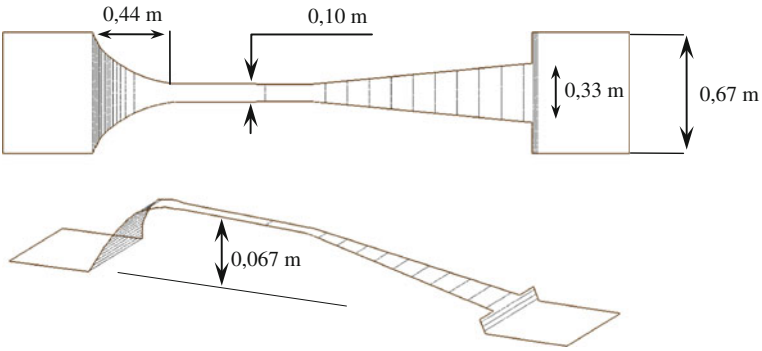

Fig. 3 Geometry of the Venturi flume used in the experiment. *Top* plan view. *Bottom* bird's eye view with a vertical scale magnified by a factor 5

5 cm along the Venturi flume and up to 50 cm upstream (the free surface elevation was measured horizontally upstream of this distance).

Figure 4 (left) shows the longitudinal profile of the spectral radius of M, that is, $1 + S_{0,x}^2$ (because $S_{0,y} = 0$). Note that this profile, which is computed using an approximation of the Venturi bottom slope between two measurement points, is an experimental profile. It can bee seen that $1 + S_{0,x}^2$ is significantly larger than unity upstream of the narrow section. The free surface elevation profile may thus be expected to be significantly different from that given by the classical shallow water equations in the upstream part of the Venturi flume, while no significant difference should be expected in the narrow and downstream parts.

The numerical solutions computed by solving both the classical and modified shallow water equations are compared to the experimental free surface profiles in Fig. 4 (right). It can be seen that under steady conditions, very little difference is observed between the two numerical solutions. The difference between the simulated and computed free surface elevations in the narrow section of the Venturi

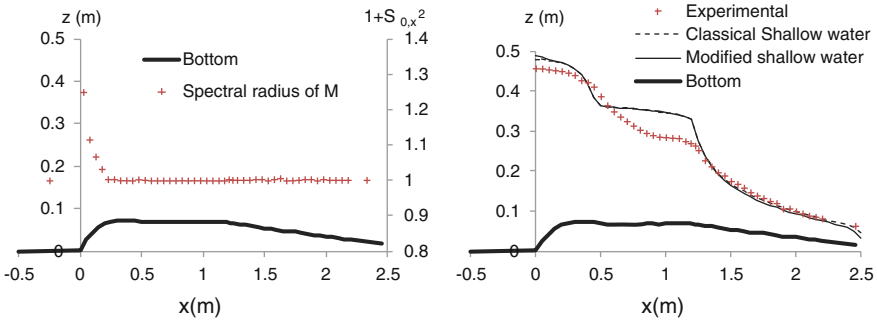

Fig. 4 Venturi flume. *Left* spectral radius of the mass/inertia matrix M as a function of the longitudinal coordinate. *Right* bottom and free surface profiles for a steady discharge $Q = 40$ L s^{-1}

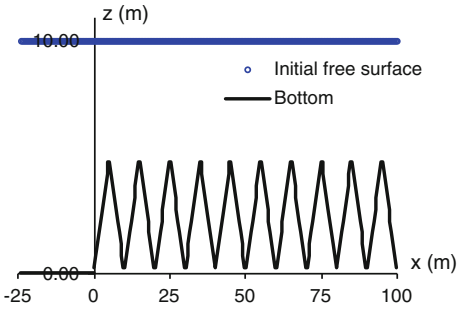

Fig. 5 Transient propagation over undulated *bottom*. Longitudinal profile of the *bottom* and initial free surface

flume is clearly due to non-hydrostatic pressure distribution stemming from the strong vertical accelerations. However, these accelerations are mainly due to the curvature of the free surface, not to the bottom gradient.

4.2 Transient Propagation over Undulated Bottom

In this test, a transient propagates into still water over a sawtooth-shaped bottom (Fig. 5). The length and height of the bottom undulations are, respectively, 10 and 5 m, which means that the bottom slope is $\pm$ 45°. At $t = 0$, $z_s = 10$ m and $u = v = 0$ m s^{-1}. At $t > 0$, a constant unit discharge $q_b = 1$ m^2 s^{-1} is injected at the left-hand boundary of the model. This creates a moving bore that propagates to the right along the x-direction. When the bore reaches the sawtooth-shaped bottom, part of the transient continues to the right, while part of it is reflected back to the left. In simulating this type of transient (shock wave), a proper formulation of the equations in conservation form is essential.

Figure 6 shows the simulated free surface elevations at various times using the classical, hydrostatic, and non-hydrostatic shallow water Eq. (11). As predicted in [1, 4], the two models are equivalent as long as the transient propagates over zero bottom slopes (which is the case for $x < 0$ m and $t < 5$ s), while the non-hydrostatic model exhibits slower wave propagation speeds when the bottom slope is non-zero; hence; the larger free surface elevations are observed compared to the hydrostatic shallow water model.

5 Conclusions

A shock-capturing, finite volume implementation, has been presented for the non-hydrostatic shallow water equations of [1, 4]. The governing equations in conservation form are easy to implement in the framework of classical time-stepping procedures.

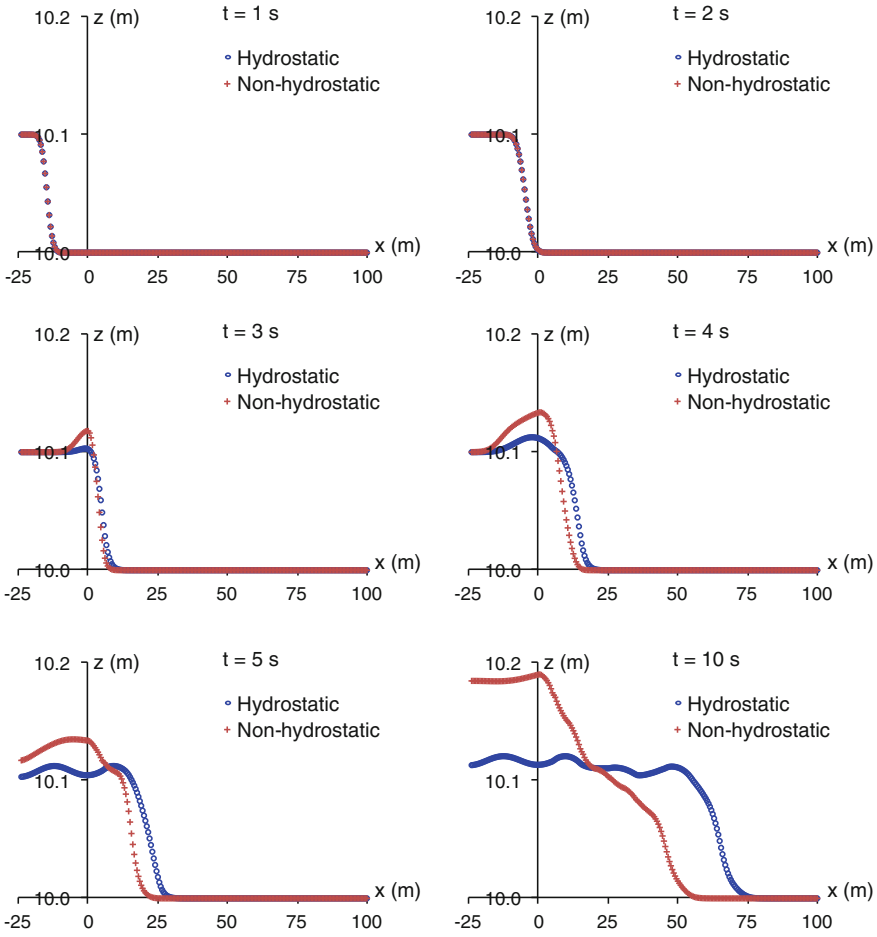

Fig. 6 Transient propagation over sawtooth-shaped *bottom*. Simulated water depths at various times

Computational applications seem to indicate that the non-hydrostatic model does not bring significant differences compared to the hydrostatic model when steady flows are involved. In contrast, transient propagation seems to be more strongly influenced by the hydrostatic/non-hydrostatic assumption. Experimental validation is obviously needed to confirm the added value brought by this model.

References

1. Clamond, D., & Dutykh, D. (2012). Practical use of variational principles for modelling water waves. *Physica D: Nonlinear Phenomena, 241*, 25–36.
2. Radder, A. C. (1999). Hamiltonian dynamics of water waves. *Advances in Coastal and Ocean Engineering, 4*, 21–59.
3. Salmon, R. (1988). Hamiltonian fluid mechanics. *Annual Review of Fluid Mechanics, 20*, 225–256.
4. Dutykh, D., & Clamond, D. (2011). Shallow water equations for large bathymetry variations. *Journal of Physics A: Mathematical and Theoretical, 44*, 332001.
5. Stoker, J.J. (1957). Water waves. Interscience.
6. Finaud-Guyot, P., Delenne, C., Lhomme, J., Guinot, V., & Llovel, C. (2010). An approximate-state Riemann solver for the two-dimensional shallow water equations with porosity. *International Journal for Numerical Methods in Fluids, 62*, 1299–1331.
7. Guinot, V., & Soares-Frazão, S. (2006). Flux and source term discretization for shallow water models with porosity on unstructured grids. *International Journal for Numerical Methods in Fluids, 50*, 309–345.
8. Guinot, V. (2012). Multiple porosity shallow water models for macroscopic modelling of urban floods. *Advances in Water Resources, 37*, 40–72.
9. Guinot, V., Delenne, C., & Cappelaere, B. (2009). An approximate Riemann solver for sensitivity equations with discontinuous solutions. *Advances in Water Resources, 32*, 61–77.
10. Van Leer, B. (1977). Toward the ultimate conservative difference scheme. IV. A new approach to numerical convection. *Journal of Computational Physics, 23*, 276–299.
11. Soares-Frazão, S., & Guinot, V. (2007). An eigenvector-based linear reconstruction scheme for the shallow water equations on two-dimensional unstructured meshes. *International Journal for Numerical Methods in Fluids, 53*, 23–55.
12. Toro, E. F., Spruce, M., & Speares, W. (1994). Restoration of the contact surface in the HLL-Riemann solver. *Shock Waves, 4*, 25–34.
13. Guinot, V. (2010). *Wave propagation in fluids. Models and numerical techniques*. 2nd edition. Wiley-ISTE.